IEEE Access
Multidisciplinary | Rapid Review | Open Access Journal

Received August 7, 2020, accepted August 20, 2020, date of publication September 1, 2020, date of current version September 15, 2020.

Digital Object Identifier 10.1109/ACCESS.2020.3020878

Field Demonstrations of Wide-Beam Optical Communications Through Water–Air Interface

XIAOBIN SUN[1], (Member, IEEE), MEIWEI KONG[1], (Member, IEEE), OMAR ALKHAZRAGI[1], (Graduate Student Member, IEEE), KUAT TELEGENOV[2], MUSTAPHA OUHSSAIN[3], MOHAMMED SAIT[1], (Graduate Student Member, IEEE), YUJIAN GUO[1], (Graduate Student Member, IEEE), BURTON H. JONES[3], JEFF S. SHAMMA[2], (Fellow, IEEE), TIEN KHEE NG[1], (Senior Member, IEEE), AND BOON S. OOI[1], (Senior Member, IEEE)

[1]Photonics Laboratory, Division of Computer, Electrical, and Mathematical Sciences and Engineering, King Abdullah University of Science and Technology (KAUST), Thuwal 23955-6900, Saudi Arabia
[2]Robotics, Intelligent Systems and Control Laboratory, Computer, Electrical and Mathematical Science and Engineering (CEMSE) Division, King Abdullah University of Science and Technology (KAUST), Thuwal 23955-6900, Saudi Arabia
[3]Integrated Ocean Processes Laboratory, King Abdullah University of Science and Technology (KAUST), Thuwal 23955-6900, Saudi Arabia

Corresponding author: Boon S. Ooi (boon.ooi@kaust.edu.sa)

This work was supported in part by the King Abdullah University of Science and Technology (KAUST) under Grant BAS/1/1614-01-01, Grant KCR/1/2081-01-01, Grant KCR/1/4114-01-01, Grant GEN/1/6607-01-01, and Grant FCC/1/1973-27-01.

ABSTRACT The connectivity of undersea sensors and airborne nodes across the water–air interface has been long sought. This study designs a free-space wireless laser communications system that yields a high net data rate of 850 Mbit/s when perfectly aligned. This system can also be used for an extended coverage of 1963 cm^2 at the receiver while sustaining a net data rate of 9 Mbit/s over 10 m. The utility of this system was verified for direct communications across the water–air interface in a canal of the Red Sea based on a pre-aligned link as well as a diving pool under a mobile signal-searching mode. The canal deployment measured a real-time data rate of 87 Mbit/s when pre-aligned in turbid water over 50 min, which confirms the system robustness in harsh water environments. In the pool deployment, a drone configured with a photodetector flew over the surface of the water and recorded the underwater signals without a structure-assisted alignment. Using a four-quadrature amplitude-modulated orthogonal frequency-division multiplexing (4-QAM-OFDM) modulation scheme provided a net data rate of 44 Mbit/s over a 2.3-m underwater and 3.5-m air link. The results validated the link stability and mitigated problems that arise from misalignment and mobility in harsh environments, which paves the way for future field applications.

INDEX TERMS Underwater communication, optical modulation, wireless communications, water-to-air communications, cross-medium communications, mobility.

I. INTRODUCTION

The concept of the Internet of Underwater Things (IoUT) was proposed in 2012 to satisfy the demands of underwater communication networks [1]. The wide, license-free bandwidth and low energy consumption in such environments promote the consideration of underwater wireless optical communication (UWOC) as a transformative technology compared with conventional marine acoustic and radio-frequency (RF) technologies for high-speed communication activities in the IoUT. Verifications of the UWOC physical layer are progressing rapidly [2], with multiple Gbit/s-level UWOC links reported in laboratory studies [3]–[8]. Beyond investigations under ideal laboratory environments, researchers have considered the effects of various natural underwater processes on the performance of UWOC links. Bubbles [9], waves [10], aquatic life [11], water turbidity [12], and oceanic turbulence [13] all degrade communication performance in UWOC by altering the path of light propagation and by inducing misalignment.

The difficulty of obtaining precise position, acquisition, and tracking (PAT) information in submerged oceanic

The associate editor coordinating the review of this manuscript and approving it for publication was Barbara Masini.

This work is licensed under a Creative Commons Attribution 4.0 License. For more information, see https://creativecommons.org/licenses/by/4.0/

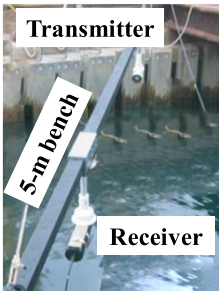

14.4 kbit/s at 3.7 m,
in the dock, WHOI
Bench aligned (2004)
(a)

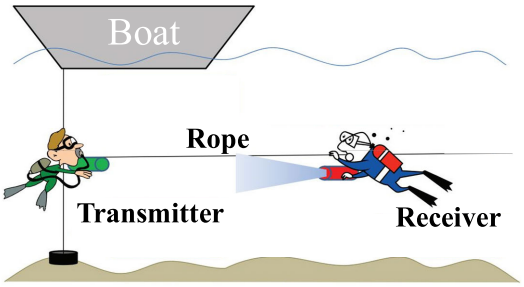

AquaOptical:0.6 Mbit/s at 9.5 m,
in the Singapore Harbor, MIT & NUS
Rope aligned (2009)
(b)

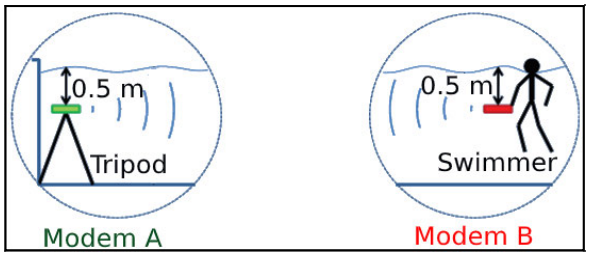

AquaOptical II: 2.28 Mbit/s at 50 m,
in Olympic-sized pool, MIT
Swimmer aligned (2010)
(c)

8.7 Mbit/s at 7.8 m,
in Narragansett Bay, RI, MIT
Framework aligned (2017)
(d)

FIGURE 1. **(a) Woods Hole Oceanographic Institution (WHOI) bench-aligned UWOC system (from [14]), (b) Massachusetts Institute of Technology (MIT) & National University of Singapore (NUS) rope-aligned UWOC system (from [15]), (c) MIT swimmer-aligned UWOC system (from [16]), (d) MIT framework-aligned UWOC system (from [12]).**

environments hampers undersea missions when using optical light. To address this problem, various structure-assisted pre-alignment methods have been used in UWOC field demonstrations [12], [14]–[16], which have yielded data rates that range from several kbit/s to a few Mbit/s, as summarized in Fig. 1. Regardless of these field trials, the cumbersome alignment structures and low dataset exfiltration rates limit the practicality of such links. Researchers are pursuing the complementary goals of both relieving the alignment requirements and increasing the data throughput of undersea optical communication links. One of the target applications of these links, which is considered in this study, is direct optical transmission through the water-air interface for connectivity between undersea and airborne vehicles.

Direct communication across the water–air interface has been a long sought but challenging achievement. Conventional acoustic waves [17] mostly reflect off the water surface without transmitting, whereas RF waves rapidly decay in water because of their high attenuation [18]. State-of-the-art workarounds for this problem have been proposed in [10] using relay assets [19], surfacing, integrated acoustic RF wireless systems (translational acoustic RF (TARF) communications, MIT, 2019) [20], and line-of-sight (LOS) optical links [7], [21], [22]. However, relay and surfacing involve large signal delays and security concerns, respectively, while TARF suffers from low data rates (400 bit/s). Furthermore, LOS optical links are vulnerable due to the difficulty of maintaining PAT. New system configurations that improve anti-jamming capabilities [12] are also in demand. King Abdullah University of Science & Technology's (KAUST) Photonics Laboratory recently developed a 110 Mbit/s diffuse-line-of-sight (diffuse-LOS) optical communication link across a wavy water–air interface that showed good coverage and was resilient to misalignment [10]. Fig. 2 compares the limitations in the performances of different schemes for communications across the water–air interface.

Despite their promising laboratory results, the above links require further investigation in actual ocean environments to determine their practicality. In this study, a laser-based, diffuse-LOS optical communication link is designed with a wide coverage of $\sim$1963 cm^2 at a data rate of 9 Mbit/s, a high speed of 850 Mbit/s when perfectly aligned, and a long transmission distance of 10 m in free space. The practical implementation of this link was tested in a canal of the Red Sea, which features high water turbidity and large waves. The communication performance was measured over 50 min at a rate of 87 Mbit/s at 1.5 m below the water and 1 m in the air

given the in-situ water quality. To the best of our knowledge, this is the first sea trial of a communication system of this kind across a wavy water–air interface. While typical optical links are constrained to operate between local terminals, our proposed link was also verified over a mobile signal searching mode using a drone-mounted photodetector. A net data rate of 44 Mbit/s with a transmission length at 2.3 m underwater and 3.5 m in the air was achieved for communications between fixed underwater nodes and mobile airborne nodes. Collectively, these results reflect impressive performance for direct communications across a wavy water–air interface in a mobile signal search mode.

II. DESIGN OF FREE-SPACE LABORATORY SYSTEM

The proposed diffuse-LOS link design is shown in Fig. 2(e), which uses a divergent laser diode (LD) beam. There is an inherent tradeoff between the overall coverage area in air and the power density at the receiver plane. The divergence angle of the laser, θ_e, and its divergence angle in air, θ_r, are related through Snell's law. As the water has a higher refractive index, the divergence in the air is larger than that underwater when assuming a flat interface. In the presence of waves, a narrow beam randomly diverges and the signal is lost. However, a divergent initial beam has an improved stability in this case. It is noted that within the divergence angle of the beam, some light rays could not penetrate through the water-air interface when the incident angle θ_i is greater than the critical angle θ_c for total internal reflection (TIR). The coverage and light rays of such links could be modeled and calculated based on the divergence angle of the laser beam, transmission distance, and Snell's laws with a surface model. The surface models include the Boussinesq equations and Korteweg-de Vries equation (KdV) for shallow water [23] and Stokes' wave theory applied for intermediate and deeper waters [24]. Deep water is defined as depths that are much larger than the wave period. A comprehensive simulation study previously analyzed the coverage and light intensity for a communication link from air-to-water across a wavy water-air interface [25]. However, additional power loss caused by TIR should be considered for light beams that propagate from water to air. Moreover, the beam expands as it travels from water to air, which is unlike the case considered in [25]. Our focus here is to experimentally demonstrate the water-to-air link and validate its practicality in realistic scenarios.

The comparatively low attenuation coefficient of blue-green light in water [11] allowed using a white-light laser (SaNoor Technologies, SNWL-3A) with a short-pass filter (SPF) (cut-off wavelength of 500 nm) as the transmitter. Fig. 3 shows the basic properties of the transmitter. The light–output–current–voltage (L–I–V) curve of the phosphor-converted white-light laser is shown in Fig. 3(a). A driving current of 0.57 A was injected into the laser diode to bias it in the linear region. Fig. 3(b) shows the spectrum of the

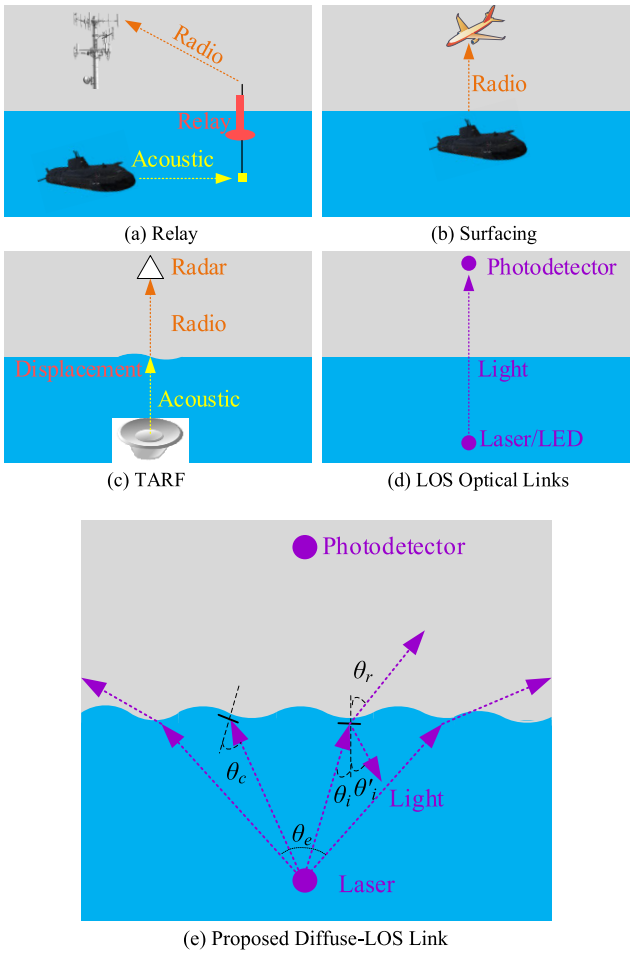

FIGURE 2. Available methods for direct/indirect communications across the wate–air interface, including (a) relays, (b) surfacing, (c) translational acoustic RF (TARF), (d) LOS optical links, and (e) the proposed laser-based diffuse-LOS link.

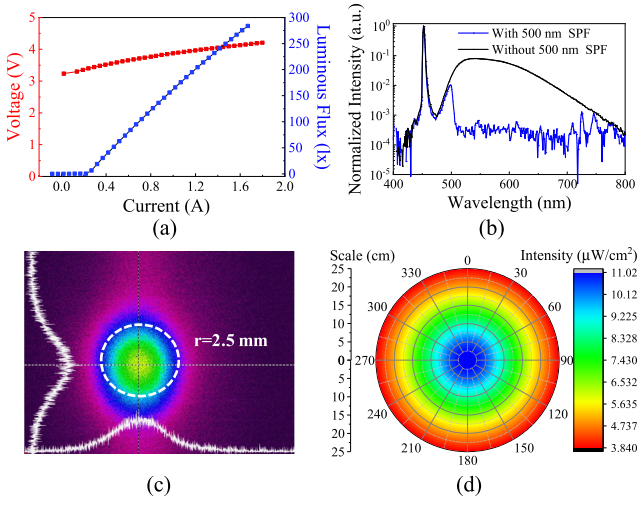

FIGURE 3. (a) L–I–V characteristics of the phosphor-converted white laser, (b) optical spectrum of the white light laser with a driving current of 570 mA with/without a 500 nm short-pass filter (SPF), (c) beam shape and power distribution of the laser, and (d) illumination distribution at a distance of 10 m.

white-light laser with and without the 500-nm SPF. It is evident from the 450-nm peak in the laser spectrum without the SPF that the white light was generated from a 450-nm excitation laser and a broadband emission phosphor. The sudden drop in intensity at 500 nm in the spectrum with the SPF shows that it blocked the out-band light. As shown in Fig. 3(c), the laser had a circular beam with a Gaussian distribution for illumination power both vertically and horizontally. This circularly symmetric beam profile led to an easier signal search in the deployed photodetector, which could detect the signal in air from any direction. Fig. 3(d) shows the power distribution of the beam with the SPF at a transmission distance of 10 m, where a circular illumination area with a diameter of ∼50 cm was formed at a divergence angle of 2.9 degrees. A maximum light intensity of 11.2 μW/cm^2 was recorded at the center of the coverage, indicating a weak light detection capability.

Fig. 4 shows the frequency response of the diode laser after propagating 10 m. The photodetector used to measure the frequency response was an APD210 (Menlo Systems, -3 dB bandwidth: 1 GHz, and spectral responsivity: 5 A/W at 450 nm). With the SPF, the bandwidth of the diode laser was significantly enhanced to over 1 GHz, compared with a few tens of MHz without the SPF. This can be explained by the slow phosphor conversion caused by the long lifetime of its excitation state, which is usually on the order of microseconds. As a result, the bandwidth of the phosphor-associated laser is limited to a few MHz in unfiltered systems [26]. Therefore, we installed the SPF before the diode laser in the system design.

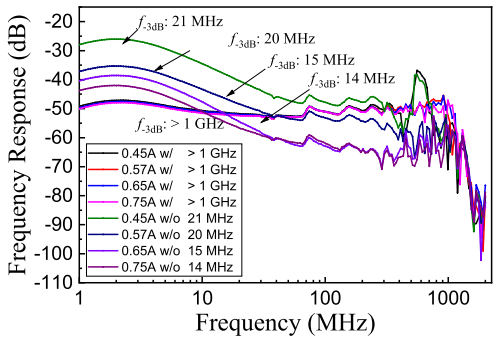

FIGURE 4. The frequency response of the entire system as measured at a transmission distance of 10 m under different driving currents with (w/)/without (w/o) a 500-nm SPF.

Fig. 5 shows the experimental setup of the laser and the avalanche photodetector (APD)-based 10-m diffuse-LOS communication system. To simultaneously maximize the achievable data rates and enhance the resiliency to channel uncertainty, amplitude-modulated orthogonal frequency-division multiplexing (QAM-OFDM) modulated signals were utilized in the system. Furthermore, our previous studies [10] indicated that the low signal-to-noise ratio (SNR) requirements and the ability to mitigate intersymbol interference (ISI) can be achieved using lower order QAM-OFDM

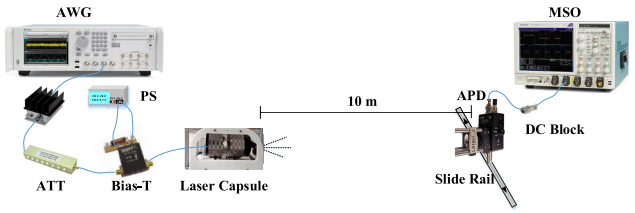

FIGURE 5. Experimental setup of the laser and APD-based wide coverage 10-m diffuse-LOS communication system. AWG: arbitrary waveform generator; AMP: amplifier; ATT: attenuator; PS: power supply; APD: avalanche photodetector; and MSO: mixed-signal oscilloscope.

modulation schemes based on three key performance matrices: data rates, robustness against waves, and communication coverage. In this system, the QAM-OFDM modulations with a high spectral efficiency were generated offline in MATLAB and uploaded to an arbitrary waveform generator (AWG, Tektronix AWG70002A). The amplitude of the signal output from the AWG was 0.5 V. The parameters of the QAM-OFDM signals used in this study are given in Table 1.

TABLE 1. Main parameters of the diffuse-LOS system using QAM-OFDM.

Parameters	Values							
Gross data rate[1]	976	900	700	500	300	100	50	10
Net data rate[2]	850	783	610	436	261	87	44	9
Coverage[3]	Alignment required			19.6	78.5	314	707	1964
Number of subcarriers	200	368	286	205	123	204	102	41
QAM size	16	4						
Sampling rate of AWG[4]	1250					250		125
Sampling rate of MSO[5]	6250					1250		625
Number of OFDM symbols[6]	100							200
IFFT size	1024							
Number of cyclic prefix	10							
Number of subcarriers for gap	2							

[1,2]Units for the gross data rate and net data rate are Mbit/s
[3]The units for the coverage is cm^2
[4,5]The units for the sampling rate of AWG and MSO are Msample/s
[6]The symbols including two training symbols and four training symbols for timing synchronization and channel equalization, respectively.

The net data rates listed in Table 1 exclude the effects of the cyclic prefix (CP), forward error correction (FEC) overhead of 7%, and training symbols for channel equalization. The signals were then transmitted through a 25-dB amplifier (AMP, Mini-Circuits ZHL-6A+) and a key-press variable attenuator (ATT, KT2.5-60/1S-2S). The ATT was used to adjust the amplitude of the signals to be within the linear operating regime of the laser. Following this, the signals were superimposed with a direct current (DC) of 570 mA on the laser using a bias tee (Bias-T, Tektronix PSPL5580). For consistency with empirical systems deployed underwater, the laser tested in this stage was mounted in a sealed laser capsule. An APD (Thorlabs APD430A2/M, -3 dB bandwidth of 400 MHz, and spectral responsivity of 32 A/W at 450 nm) was 10 m from the transmitter with a focusing lens (LA1027-A) mounted on a slide rail to scan the signal coverage. The signal was output to a mixed-signal oscilloscope

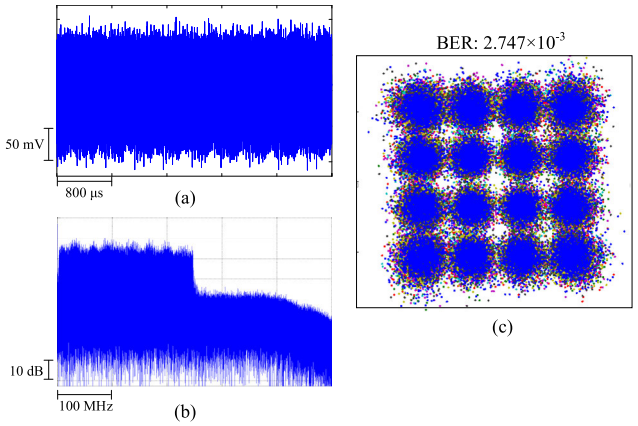

FIGURE 6. (a) Waveform, (b) spectrum, and (c) constellation map (bit error ratio (BER) of 2.747 × 10^{-3}) of the captured 976-Mbit/s 16-QAM-OFDM signal at a transmission distance of 10 m.

(MSO, Tektronix DPO72004C) after filtering the DC component using a DC block. The APD430A2 was used because it has a significantly higher responsivity at 450 nm than the APD210 used to measure the bandwidth. The higher responsivity offered a larger SNR, which is more suitable for underwater deployment in dynamic environments.

A maximum gross data rate of 976 Mbit/s was achieved when aligned and using the 16-QAM-OFDM modulation. Fig. 6(a) shows the waveform of the captured OFDM signal in the time domain and Fig. 6(b) shows the corresponding spectrum in the frequency domain. The scales of the vertical and horizontal axes are given in the figure. As shown in Fig. 6(b), the signal occupied a bandwidth of 244 MHz. Fig. 6(c) shows the constellation diagram of the received signal, indicating a bit error ratio (BER) of 2.747 × 10^{-3}.

We employed a 4-QAM-OFDM modulation scheme to investigate the maximum coverage of the system, which requires a lower SNR than other higher-order QAM-OFDM schemes. The data capacity of this system with the 4-QAM-OFDM was first tested by measuring the BERs against the data rates when aligned. As shown in Fig. 7(a), a maximum data rate of 900 Mbit/s with a BER below the FEC limit (3.8 × 10^{-3}) was obtained using the 4-QAM-OFDM. The insets (i), (ii), and (iii) of Fig. 7(a) show the constellations for the gross data rates of 500, 700, and 900 Mbit/s, respectively. It is seen that more convergent constellations occurred at the lower data rates. We then measured the coverage of the data capacity for the 4-QAM-OFDM modulated system. The APD moved from the aligned to off-aligned positions in steps of 2.5 cm using a slide rail. The BERs at different positions were measured as a reference to determine the coverage of the system at specific data rates.

As observed in Fig. 7(b), alignment was required for gross data rates above 700 Mbit/s to ensure that the BERs were lower than the FEC limit. However, for gross data rates below 700 Mbit/s, the system began to tolerate misalignments. Moreover, the coverage increased with smaller data

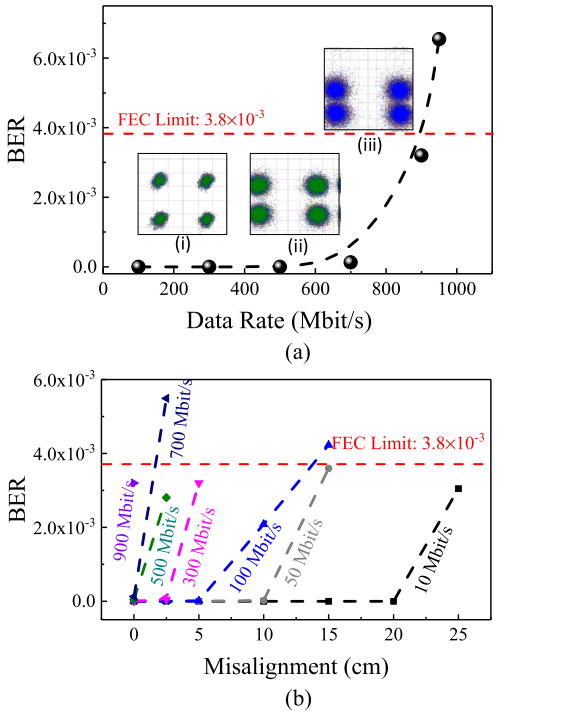

FIGURE 7. (a) BERs vs. gross data rates using a 4-QAM-OFDM at the aligned position with a transmission distance of 10 m. Insets (i), (ii), and (iii) are the constellations for gross data rates of 500, 700, and 900 Mbit/s, respectively. (b) The BERs vs. misalignment for different gross data rates (10, 50, 100, 300, 500, 700, and 900 Mbit/s) with a transmission distance of 10 m using the 4-QAM-OFDM.

rates. For a gross data rate of 10 Mbit/s, a misalignment of 25 cm is still acceptable with a corresponding BER of 3.05 × 10^{-3}. The circular symmetry of the power distribution for the beam provided a coverage of ∼1963 cm^2 at this data rate. Similarly, coverages at all data rates were calculated and are summarized in Fig. 8.

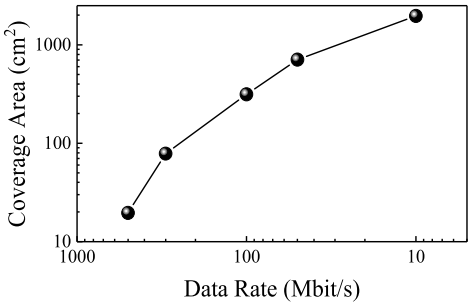

FIGURE 8. The respective coverages for different gross data rates (10, 50, 100, 300, and 500 Mbit/s) with a transmission distance of 10 m using the 4-QAM-OFDM. Gross data rates of 700 Mbit/s and above require strict alignment to ensure effective communication links.

III. PRE-ALIGNED DEPLOYMENT IN RED SEA CANAL

To investigate the performance of the proposed system for communications across the water–air interface, we deployed it in the Red Sea for in-ocean testing at a canal facility at KAUST. The measurements were made at 6:00 PM,

FIGURE 9. Location of the in-ocean testing for communications across the water–air interface at a canal facility at KAUST.

on November 20, 2019, GMT+3 at the testing location shown in Fig. 9. The satellite photo indicates that the water turbidity in the canal and the harbor was much higher than that of the open ocean.

Our experimental configuration to deploy the proposed communication system in a canal of the Red Sea across the water–air interface is shown in Fig. 10(a). The photodetector was mounted on a slide rail 1 m above the water surface. Fig. 10(b) shows a photo of the underwater transmitter capsule, which was fixed with four ropes placed close to the canal wall. The divergent optical beam was sent upwards through a transparent acrylic window. We also measured the real-time water quality to determine the attenuation per unit length (parameter c) over time, as shown in Fig. 10(c). This was done using a WET Labs ACS hyper-spectral spectrophotometer at the same depth as the laser. Water was passed through the two tubes of the ACS using a submerged pump. The ACS instrument provided rates for spectral absorption and attenuation at 81 wavelengths from 400 to 740 nm. This method has been previously used to measure the inherent optical properties (IOPs) of the Red Sea [27]. We recorded

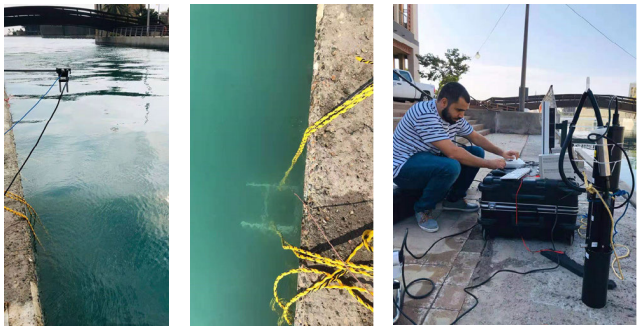

(a) (b) (c)

FIGURE 10. (a) Field apparatus for communications across the water–air interface in a turbid canal. The photodetector is mounted on a slide rail, with a height of 1 m above the water surface, (b) the photo of the laser capsule is immersed into the canal water at a depth of 1.5 m, and (c) real-time water quality measurement system.

the communication performance and water quality at a wavelength of 450 nm for 50 min.

A simulation was performed to theoretically analyze the system. Assuming the received intensity in free space is I_o, the intensity in the water-to-air configuration (assuming the free-space attenuation is negligible) is attenuated by a factor of $\exp(-cd_w)$, where c is the attenuation coefficient and d_w is the traveled distance in water (1.5 m). The signal amplitude is directly proportional to the intensity through the responsivity and the load resistance, and the SNR is proportional to the square of the amplitude. If we assume the SNR of the free-space link ($c = 0$) is $\mathrm{SNR_o}$, the SNR in the water-to-air link is expressed as:

$$SNR = SNR_o(e^{-cd_w})^2. \tag{1}$$

For 4-QAM signals, the symbol error probability is given by [28]:

$$P_s = 2Q(\sqrt{SNR}) - Q^2(\sqrt{SNR}). \tag{2}$$

where $Q(\cdot)$ is the Gaussian Q-function, and the BER is approximated by dividing P_s by $\log_2 4 = 2$ when assuming Gray coding. Fig. 11 shows the simulated BER for different $\mathrm{SNR_o}$ values.

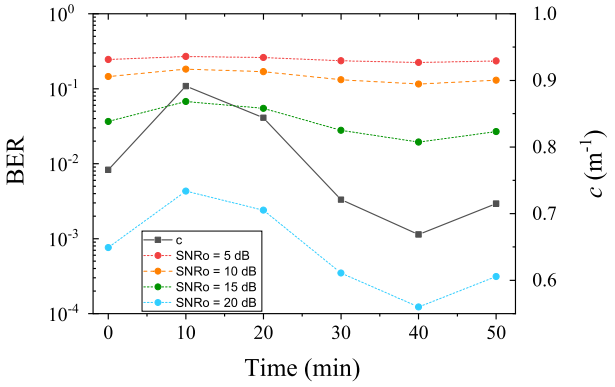

FIGURE 11. The simulated BER for different $\mathrm{SNR_o}$ values against the water attenuation coefficient for 50 min.

The results of the in-situ water quality measurements and communications experiment during the field trial are summarized in Fig. 12. The average attenuation coefficient from the canal water was 0.8 $\mathrm{m^{-1}}$, which suggests that water in the Red Sea canal at this testing spot was Jerlov Harbor I water [29]. In this study, a 4-QAM-OFDM signal with a gross data rate of 100 Mbit/s (net: 87 Mbit/s) was transmitted, which is compatible with the requirements of 8K video. The transmitter capsule was 1.5 m underwater, and the receiver was in the air 1 m above the water surface. Moving the photodetector with a slide rail allowed aligning it with the underwater transmitter. Continuously moving waves and varying attenuation coefficients led to a fluctuating amplitude for the received signal from a small signal amplitude (SSA) to a medium signal amplitude (MSA) and a large signal amplitude (LSA).

As LSA signals have a higher SNR than MSA and SSA, these were assumed to deliver the most reliable performance.

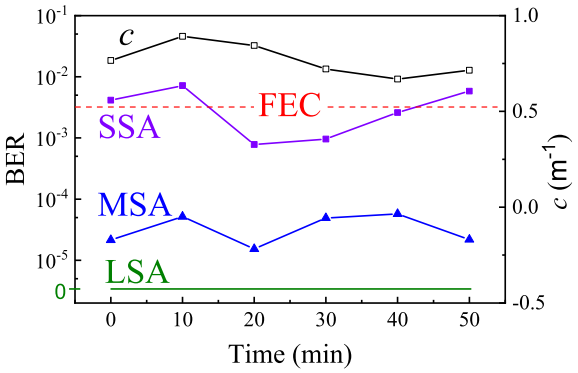

FIGURE 12. The in-situ 100 Mbit/s communication performance and the corresponding attenuation coefficients recorded for a period of 50 minutes.

This is was verified in Fig. 12, where the LSA signals always ensured an error-free, 100-Mbit/s (gross) communication link. Compared with LSA signals, the MSA signals provided a communication link with BERs in the range of 10^{-5}–10^{-4}, which is below the FEC limit. In contrast, SSA signals exhibited unstable communication performance. The BERs from 20–40 min were below the FEC limit while the others were higher. This means that 50% of the transmission corresponded to a communication outage for the SSA signals, indicating the lost data packets would need to be re-sent in empirical scenarios. This led to an effective gross data rate of 83.3 Mbit/s (considering that SSA signals occurred as frequently as the others). This is attributed to the effects of variations in the water environment and waves. The tendency of BERs for SSA signals was similar to changes in the attenuation coefficient and simulated BERs, while the deviations are attributed to surface waves. This suggests that our experimental results verified the correctness of the system design.

Collectively, the in-ocean performance was achieved at a high water turbidity and current, and the waves posed significant challenges to communications across the water–air interface. An error-free link with a gross data rate of 100 Mbit/s was implemented by collecting and decoding LSA signals. These results show that diffuse-LOS optical wireless links can be used as an alternative to direct communications across water–air interfaces.

IV. DEPLOYMENT OF MOBILE SIGNAL SEARCH IN DIVING POOL

We tested our hardware in a diving pool at KAUST in Saudi Arabia to examine the system performance in a mobile signal search mode. The attenuation coefficient of the pool water was 0.37 m^{-1}, and the water was relatively calm. These parameters suggest that water in the diving pool was Jerlov coastal water [29]. To avoid optical power attenuation due to phosphor, we directly used a blue laser diode instead of a white laser with a 500-nm SPF. The blue laser with a thermoelectric cooler (TEC) set was mounted in a sealed capsule and sent the optical beam through a clear acrylic end-cap. The signal and power of the laser were injected through a 5-m coaxial RF cable and a 5-m power cable, respectively. The APD was mounted on a drone with a 10-m coaxial RF-cable to transmit the received signal to the MSO. Two compact batteries were combined and mounted on the drone to power the APD. The drone flew over the water surface with coarse positioning to record the signal. A gross data rate of 50 Mbit/s (net: 44 Mbit/s) with the 4-QAM-OFDM signal was transmitted using this system.

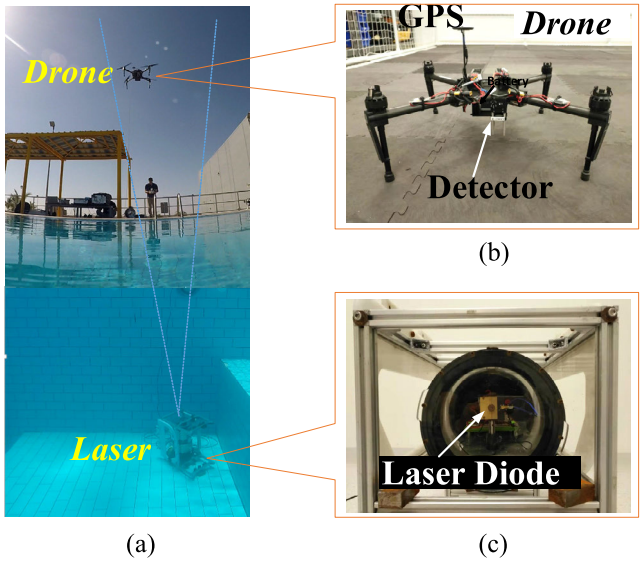

FIGURE 13. (a) A photograph of the drone-aided pool deployment apparatus, (b) APD430A2/M receiver mounted on a drone, and (c) transmitter laser mounted in the capsule.

Fig. 13(a) shows a photograph of the deployed system. The depth of the underwater transmitter was 2.3 m, and it sent a divergent optical beam upwards. After propagating through the water, water–air interface, and air, the signal was captured by an APD mounted on the drone, which hovered 3.5 m above the water and was controlled from onshore. Fig. 13(b) shows a photograph of the drone, which was a DJI MATRICE 100 with a maximum takeoff weight of 3.6 kg. The drone itself weighed 2.355 kg, which left 1.245 kg for the payload. Thus, a compact power-saving photodetector was required. Furthermore, the accuracies of the vertical and horizontal hovering based on a global positioning system (GPS) were 0.5 m and 2.5 m, respectively [30], which means that only coarse positioning was achieved by the system. The drone only has a short hover time of 17 min, so easy signal detection in the presence of drone mobility is essential. The drone was piloted by the operator in the Position Mode, which means that the drone actively braked, leveled, and was locked to a 3D spatial position to compensate for wind and other disturbances [31]. The pilot visually localized the laser beam and navigated and hovered the drone over the beam to allow for communications between the laser and sensor. Fig. 13(c) shows a photograph of the laser in the capsule as installed

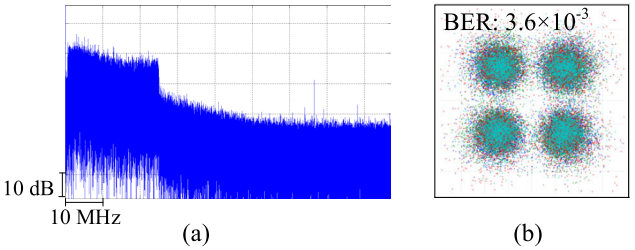

FIGURE 14. **(a) Spectrum of the captured 4-QAM-OFDM signal from the drone with a transmission distance of 2.3 m underwater and 3.5 m in the air, and (b) constellation diagram of the captured 4-QAM-OFDM signal from the drone showing a BER of 3.6×10^{-3}.**

using a frame. Iron weights were used to help sink and stabilize the capsule in the water.

Fig. 14(a) shows the spectrum of the captured 4-QAM-OFDM signal where the occupied bandwidth was 25 MHz. The link-related limitations caused the attenuation in the high-frequency subcarriers to gradually increase, which can be explained from water attenuation and link misalignment. Fig. 14(b) shows the constellation diagram of the received signal, which indicates a BER of 3.6×10^{-3}. Therefore, we successfully implemented a compact, power-saving, structure-assisted, and alignment-free communication link across the water–air interface in the presence of receiver mobility.

V. CONCLUSION

This paper designed and tested a high-speed system for direct communications across a water–air interface featuring requirements related to alignment and user mobility. The system implemented a 10-m free-space diffuse-LOS optical wireless communication link with a large coverage area of $\sim$1963 cm^2 at a gross data rate of 10 Mbit/s. A high data rate of 850 Mbit/s was achieved when perfectly aligned. The utility of the system was proven from a series of field trials and was deployed in a Red Sea canal to test its real-time communication performance over 50 min. Thus, the system exhibits strong robustness in harsh underwater environments. Furthermore, a drone-aided diving pool trial showed that the system can facilitate a 44-Mbit/s direct and mobile communication link over a transmission distance of 2.3 m under water and 3.5 m in air, which was free of structure-assisted alignment. The results suggest that QAM-OFDM-modulated diffuse-LOS optical links, which feature large signal coverage, can overcome the ISI from channel uncertainty and is favorable in harsh environments for stable communications. Such harsh environments could include turbulent underwater/atmospheric channels and communication links comprised of mobile nodes. One application is a direct communication across the water–air interface in the presence of surface waves and mobility. To the best of our knowledge, this is the first field demonstration of direct wireless optical communications across a water–air interface with the highest data rate ever reported in the literature. Our future research in this area will feature more and varied field trials.

ACKNOWLEDGMENT

The authors thank Mr. Nabeel M. Moamenah and the team at Residential and Facilities Operations, KAUST, for providing support for the Red Sea canal deployment.

REFERENCES

[1] M. C. Domingo, "An overview of the Internet of underwater things," *J. Netw. Comput. Appl.*, vol. 35, no. 6, pp. 1879–1890, Nov. 2012.

[2] X. Sun, C. H. Kang, M. Kong, O. Alkhazragi, Y. Guo, M. Ouhssain, Y. Weng, B. H. Jones, T. K. Ng, and B. S. Ooi, "A review on practical considerations and solutions in underwater wireless optical communication," *J. Lightw. Technol.*, vol. 38, no. 2, pp. 421–431, Jan. 15, 2020.

[3] C.-Y. Li, H.-H. Lu, W.-S. Tsai, Z.-H. Wang, C.-W. Hung, C.-W. Su, and Y.-F. Lu, "A 5 m/25 Gbps underwater wireless optical communication system," *IEEE Photon. J.*, vol. 10, no. 3, Jun. 2018, Art. no. 7904909.

[4] C. Fei, X. Hong, G. Zhang, J. Du, Y. Gon, J. Evans, and S. He, "16.6 Gbps data rate for underwater wireless optical transmission with single laser diode achieved with discrete multi-tone and post nonlinear equalization," *Opt. Express*, vol. 26, no. 26, pp. 34060–34069, Dec. 2018.

[5] N. Chi, Y. Zhao, M. Shi, P. Zou, and X. Lu, "Gaussian kernel-aided deep neural network equalizer utilized in underwater PAM8 visible light communication system," *Opt. Express*, vol. 26, no. 20, pp. 26700–26712, Oct. 2018.

[6] T.-C. Wu, Y.-C. Chi, H.-Y. Wang, C.-T. Tsai, and G.-R. Lin, "Blue laser diode enables underwater communication at 12.4 gbps," *Sci. Rep.*, vol. 7, no. 1, Jan. 2017, Art. no. 40480.

[7] Y. Chen, M. Kong, T. Ali, J. Wang, R. Sarwar, J. Han, C. Guo, B. Sun, N. Deng, and J. Xu, "26 m/5.5 Gbps air-water optical wireless communication based on an OFDM-modulated 520-nm laser diode," *Opt. Express*, vol. 25, no. 13, pp. 14760–14765, Jun. 2017.

[8] F. Hanson and S. Radic, "High bandwidth underwater optical communication," *Appl. Opt*, vol. 47, no. 2, pp. 277–283, Jan. 2008.

[9] H. M. Oubei, R. T. ElAfandy, K.-H. Park, T. K. Ng, M.-S. Alouini, and B. S. Ooi, "Performance evaluation of underwater wireless optical communications links in the presence of different air bubble populations," *IEEE Photon. J.*, vol. 9, no. 2, pp. 1–9, Apr. 2017.

[10] X. Sun, M. Kong, C. Shen, C. H. Kang, T. K. Ng, and B. S. Ooi, "On the realization of across wavy water-air-interface diffuse-line-of-sight communication based on an ultraviolet emitter," *Opt. Express*, vol. 27, no. 14, pp. 19635–19649, Jul. 2019.

[11] H. M. Oubei, C. Shen, A. Kammoun, E. Zedini, K.-H. Park, X. Sun, G. Liu, C. H. Kang, T. K. Ng, and B. S. Ooi, "Light based underwater wireless communications," *Jpn. J. Appl. Phys*, vol. 57, no. 8S2, 08PA06, Jul. 2018.

[12] S. A. Hamilton, C. E. DeVoe, A. S. Fletcher, I. D. Gaschits, F. Hakimi, N. D. Hardy, T. Howe, N. Mittleman, H. G. Rao, M. S. Scheinbart, and T. M. Yarnall, "Undersea narrow-beam optical communications field demonstration," in *Proc. Ocean Sens. Monitor. IX*, Anaheim, CA, USA, vol. 10186, 2017, Art. no. 1018606.

[13] H. M. Oubei, X. Sun, T. K. Ng, O. Alkhazragi, M.-S. Alouini, and S. B. Ooi, "Scintillations of RGB laser beams in weak temperature and salinity-induced oceanic turbulence," in *Proc. 4th Underwater Commun. Netw. Conf. (UComms)*, Lerici, Italy, Aug. 2018, pp. 1–4.

[14] M. Tivey, "A low power, low cost, underwater optical communications system," in *Proc. Ridge Events*, Apr. 2004, pp. 27–29.

[15] M. Doniec, C. Detweiler, I. Vasilescu, M. Chitre, M. Hoffmann-Kuhnt, and D. Rus, "AquaOptical: A lightweight device for high-rate long-range underwater point-to-point communication," *Mar. Technol. Soc. J.*, vol. 44, no. 4, pp. 55–65, Oct. 2010.

[16] M. Doniec and D. Rus, "BiDirectional optical communication with AquaOptical II," in *Proc. IEEE Int. Conf. Commun. Syst.*, Singapore, Nov. 2010, pp. 390–394.

[17] M. Chitre, S. Shahabudeen, and M. Stojanovic, "Underwater acoustic communications and networking: Recent advances and future challenges," *Mar. Technol. Soc. J.*, vol. 42, no. 1, pp. 103–116, Mar. 2008.

[18] A. Palmeiro, M. Martín, I. Crowther, and M. Rhodes, "Underwater radio frequency communications," in *Proc. OCEANS*, Santander, Spain, Jun. 2011, pp. 1–8.

[19] I. F. Akyildiz, D. Pompili, and T. Melodia, "Underwater acoustic sensor networks: Research challenges," *Ad Hoc Netw.*, vol. 3, no. 3, pp. 257–279, May 2005.
[20] F. Tonolini and F. Adib, "Networking across boundaries: Enabling wireless communication through the water-air interface," in *Proc. Conf. ACM Special Interest Group Data Commun.*, Budapest, Hungary, Aug. 2018, pp. 117–131.
[21] K. I. Gjerstad, J. J. Stamnes, B. Hamre, J. K. Lotsberg, B. Yan, and K. Stamnes, "Monte Carlo and discrete-ordinate simulations of irradiances in the coupled atmosphere-ocean system," *Appl. Opt.*, vol. 42, no. 15, pp. 2609–2622, May 2003.
[22] R. S. Sangeetha, R. L. Awasthi, and T. Santhanakrishnan, "Design and analysis of a laser communication link between an underwater body and an air platform," in *Proc. Int. Conf. Next Gener. Intell. Syst. (ICNGIS)*, Kottayam, India, Sep. 2016, pp. 1–5.
[23] P. Rozmej, A. Karczewska, and E. Infeld, "Superposition solutions to the extended KdV equation for water surface waves," *Nonlinear Dyn.*, vol. 91, no. 2, pp. 1085–1093, Jan. 2018.
[24] R. L. Wiegel, "A presentation of cnoidal wave theory for practical application," *J. Fluid Mech.*, vol. 7, no. 2, pp. 273–286, Feb. 1960.
[25] M. S. Islam and M. F. Younis, "Analyzing visible light communication through air–water interface," *IEEE Access*, vol. 7, pp. 123830–123845, Aug. 2019.
[26] I. Dursun, C. Shen, M. R. Parida, J. Pan, S. P. Sarmah, D. Priante, N. Alyami, J. Liu, M. I. Saidaminov, M. S. Alias, A. L. Abdelhady, T. K. Ng, O. F. Mohammed, B. S. Ooi, and O. M. Bakr, "Perovskite nanocrystals as a color converter for visible light communication," *ACS Photon.*, vol. 3, no. 7, pp. 1150–1156, Jul. 2016.
[27] M. Kheireddine, M. Ouhssain, M. L. Calleja, X. A. G. Morán, Y. V. B. Sarma, S. P. Tiwari, and B. H. Jones, "Characterization of light absorption by chromophoric dissolved organic matter (CDOM) in the upper layer of the red sea," *Deep Sea Res. I, Oceanogr. Res. Papers*, vol. 133, pp. 72–84, Mar. 2018.
[28] M. K. Simon and M.-S. Alouini, "Performance of single channel receivers," in *Digital Communication Over Fading Channels*. Hoboken, NJ, USA: Wiley, Jan. 2002, pp. 193–258.
[29] N. G. Jerlov, "Irradiance optical classification," in *Optical Oceanography*, N. G. Jerlov, Ed. Amsterdam, The Netherlands: Elsevier, 1968, pp. 118–120.
[30] *DJI—The World Leader in Camera Drones/Quadcopters for Aerial Photography*. Accessed: Dec. 9, 2019. [Online]. Available: https://www.dji.com/matrice100/info
[31] *Flight Modes · PX4 User Guide*. Accessed: Dec. 9, 2019. [Online]. Available: https://docs.px4.io/master/en/getting_started/flight_modes.html

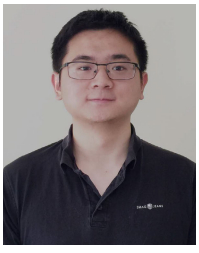

XIAOBIN SUN (Member, IEEE) received the B.S. degree in semiconductor physics from the University of Science and Technology, Beijing, in 2016, and the Ph.D. degree in optical wireless communications from the King Abdullah University of Science and Technology (KAUST), in 2020. His research interests include underwater wireless optical communications, free-space optical communications, and quantum communications.

MEIWEI KONG (Member, IEEE) received the B.S. degree in material physics from Zhejiang Normal University, China, and the Ph.D. degree in marine information science and engineering from the School of Ocean College, Zhejiang University. She is currently a Postdoctoral Researcher with the King Abdullah University of Science and Technology (KAUST). Her research interest is in underwater wireless optical communications.

OMAR ALKHAZRAGI (Graduate Student Member, IEEE) received the B.S. degree in electrical engineering from the King Fahd University of Petroleum and Minerals (KFUPM), Saudi Arabia, in 2018. He is currently pursuing the M.S./Ph.D. degree in electrophysics with the Photonics Laboratory, King Abdullah University of Science and Technology (KAUST), Saudi Arabia. The primary focus of his research is experimental and theoretical studies of optical wireless communication systems.

KUAT TELEGENOV received the B.Eng. degree in mechanical engineering from the University Technology of Malaysia and the M.Sc. degree in mechanics from the Gumilyov Eurasian National University, Kazakhstan, in 2014. He is currently a Research Scientist with the Robotics, Intelligent Systems and Control Laboratory, King Abdullah University of Science and Technology (KAUST).

MUSTAPHA OUHSSAIN received the B.Sc. degree in chemistry from Université Montpellier 2, France, in 2006, and the M.S. degree in sciences, technology and marine environments from Toulon University, Toulon, France. He is currently a Laboratory Engineer with the Red Sea Research Center, King Abdullah University of Science and Technology (KAUST). His research interests include ocean optics, analytical services, and field and laboratory analysis of marine environments.

MOHAMMED SAIT (Graduate Student Member, IEEE) is currently pursuing the Ph.D. degree with the Photonics Laboratory, Division of Computer, Electrical and Mathematical Sciences and Engineering (CEMSE), King Abdullah University of Science and Technology (KAUST). His research interests include underwater optical communications and VLC, and LiFi technology.

YUJIAN GUO (Graduate Student Member, IEEE) received the B.S. degree in electrical engineering from the University of Electronic Science and Technology of China, Chengdu, Sichuan, in 2017. He is currently pursuing the Ph.D. degree with the Department of Computer, Electrical and Mathematical Sciences and Engineering, King Abdullah University of Science and Technology (KAUST). His current research interests include underwater wireless optical communications and underwater optical channel characterization.

BURTON H. JONES received the Ph.D. degree from Duke University. He is currently a Professor of integrated ocean processes with the King Abdullah University of Science and Technology (KAUST). His current interests include biological oceanography, physical and biological interactions, ocean optics, coastal urban issues, and integrated observation and modeling.

JEFF S. SHAMMA (Fellow, IEEE) received the Ph.D. degree from the Massachusetts Institute of Technology, in 1988. He is currently a Professor of electrical engineering with the King Abdullah University of Science and Technology (KAUST). His most recent research has been in decision and control for distributed multiagent systems, and related topics in game theory and network science with applications to both cyberphysical and societal network systems.

TIEN KHEE NG (Senior Member, IEEE) received the M.Eng. and Ph.D. degrees from Nanyang Technological University (NTU), Singapore, in 2005 and 2001, respectively. He is currently a Principal Research Scientist with the King Abdullah University of Science and Technology (KAUST), and a Co-Principal-Investigator responsible for innovation in MBE-grown nanostructures and laser devices at the KACST Technology Innovation Center, KAUST. His focus is on the fundamental and applied research of wide-bandgap group-III nitrides, novel hybrid materials, and multi-functional devices to address efficient light-emitters, optical wireless communication in harsh environment, and energy harvesting. He is also a Senior Member of the OSA, and a member of SPIE, IET, and IoP.

BOON S. OOI (Senior Member, IEEE) received the B.Eng. and Ph.D. degrees in electronics and electrical engineering from the University of Glasgow. He is currently a Professor of electrical engineering with the King Abdullah University of Science and Technology (KAUST). His researches focus on the study of semiconductor lasers, LEDs, and photonic integrated circuits for applications in energy efficient lighting and visible-light communications. He is a Fellow of the Optics Express (OSA), SPIE, and IOP (U.K.). He is also an elected Fellow of the U.S. National Academy of Inventors (NAI). He is an Associate Editor of the IEEE PHOTONICS JOURNAL, *OSA*, and the *Journal of Nanophotonics* (SPIE).